Redox Chemistry

International Edition: DOI: 10.1002/anie.201916622
German Edition: DOI: 10.1002/ange.201916622

Element–Element Bond Formation upon Oxidation and Reduction

*Martin Piesch, Christian Graßl, and Manfred Scheer**

Dedicated to Professor Herbert W. Roesky on the occasion of his 85th birthday

Abstract: *The redox chemistry of $[(Cp'''Co)_2(\mu,\eta^2{:}\eta^2\text{-}E_2)_2]$ (E = P (**1**), As (**2**); Cp''' = 1,2,4-tri(tert-butyl)cyclopentadienyl) was investigated. Both compounds can be oxidized and reduced twice. That way, the monocations $[(Cp'''Co)_2(\mu,\eta^4{:}\eta^4\text{-}E_4)][X]$ (E = P, X = BF_4 (**3a**), [FAl] (**3b**); E = As, X = BF_4 (**4a**), [FAl] (**4b**)), the dications $[(Cp'''Co)_2(\mu,\eta^4{:}\eta^4\text{-}E_4)][TEF]_2$ (E = P (**5**), As (**6**)), and the monoanions $[K(18\text{-}c\text{-}6)(dme)_2][(Cp'''Co)_2(\mu,\eta^4{:}\eta^4\text{-}E_4)]$ (E = P (**7**), As (**8**)) were isolated. Further reduction of **7** leads to the dianionic complex $[K(18\text{-}c\text{-}6)(dme)_2][K(18\text{-}c\text{-}6)][(Cp'''Co)_2(\mu,\eta^3{:}\eta^3\text{-}P_4)]$ (**9**), in which the cyclo-P_4 ligand has rearranged to a chain-like P_4 ligand. Further reduction of **8** can be achieved with an excess of potassium under the formation of $[K(dme)_4][(Cp'''Co)_2(\mu,\eta^3{:}\eta^3\text{-}As_3)]$ (**10**) and the elimination of an As_1 unit. Compound **10** represents the first example of an allylic As_3 ligand incorporated into a triple-decker complex.*

Introduction

Oxidation and reduction reactions have been widely used for element–element bond formation or cleavage reactions. For example, the elemental modifications of sulfur (S_8), phosphorus (P_4 or red phosphorus), or gray arsenic can be easily degraded in reduction processes by bond cleavages to the corresponding S_6^{2-}, P^{3-}, or As^{3-} units, respectively.[1] On the other hand, oxidation reactions lead, in general, to bond formation. In the case of S_8, one new S–S bond is formed upon oxidation to S_8^{2+}, while for the oxidation of white phosphorus, an additional aggregation takes place to form a P_9^+ moiety.[2] Analogous reactivity can be observed for cyclic phosphines[3a,b] or arsines such as $^tBu_4E_4$ (E = P, As). Both compounds can be reduced and degraded to E_2 fragments by using elemental potassium.[3c,d] While this behavior is particularly true for saturated main group compounds containing lone pairs, the situation is different for unsaturated species. In this case, reduction leads in general to the population of π* orbitals and the formation of radical anions, which can result in bond formations.[4] For example, phosphinines,[4a] diboryl compounds,[4b] and (TPB)Cu^+ (TPB = tris[2-(diisopropylphosphino)phenyl]borane)[4c] form new formal one-electron bonds (P···P, B···B, and Cu···B) upon reduction. Polypnictogen ligands in the coordination sphere of transition metals also reveal interesting redox chemistry. The redox chemistry of pentaphosphaferrocene $[Cp^*Fe(\eta^5\text{-}P_5)]$[5] (Cp* = pentamethylcyclopentadienyl) was studied spectroelectrochemically by Winter and Geiger,[6] and experimentally by our group, generating one oxidized and two reduced products.[7] Depending on the reducing agent, one or two electrons can be transferred to $[Cp^*Fe(\eta^5\text{-}P_5)]$. When potassium hydride was used, a single-electron transfer occurred leading to a proposed intermediate $[Cp^*FeP_5]^-$, which dimerized to the dinuclear complex $[(Cp^*Fe)_2(\mu,\eta^4{:}\eta^4\text{-}P_{10})]^{2-}$. When elemental potassium was used in excess, the reaction gave the dianionic species $[Cp^*Fe(\eta^4\text{-}P_5)]^{2-}$ (**A**; Scheme 1). On the other hand, when thianthrenium hexafluoroantimonate was used as a strong oxidant, the dinuclear compound $[(Cp^*Fe)_2(\mu,\eta^4{:}\eta^4\text{-}P_{10})]^{2+}$ (**B**) was isolated. In these reactions, the polyphosphorus ligand in $[Cp^*Fe(\eta^5\text{-}P_5)]$ responds to the addition or withdrawal of one electron either by folding the P_5 ring or/and by forming a new external P–P bond.[7] The redox chemistry of the analogous arsenic compound $[Cp^*Fe(\eta^5\text{-}As_5)]$ leads, upon reduction, to a mixture of anionic species containing As_4, As_{10}, As_{14}, and As_{18} ligands, while all attempts

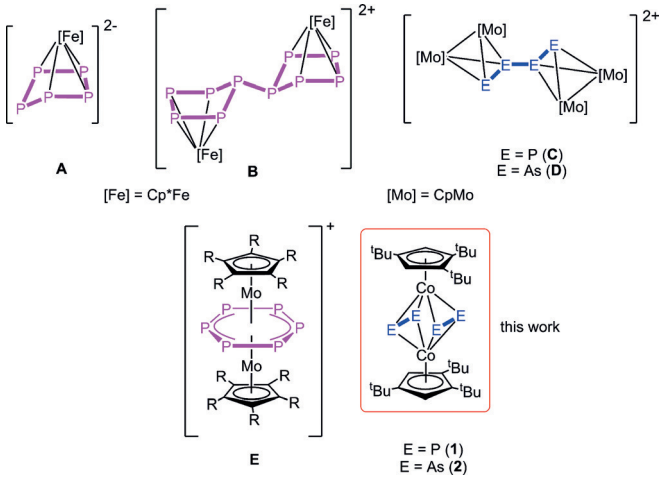

Scheme 1. Selected examples of reduced and oxidized polypnictogen ligand complexes.

[*] M. Sc. M. Piesch, Dr. C. Graßl, Prof. Dr. M. Scheer
Institut für Anorganische Chemie, Universität Regensburg
93040 Regensburg (Germany)
E-mail: Manfred.Scheer@ur.de
Homepage: https://www.uni-regensburg.de/chemie-pharmazie/anorganische-chemie-scheer/

Supporting information and the ORCID identification number(s) for the author(s) of this article can be found under: https://doi.org/10.1002/anie.201916622.

towards an oxidation have failed thus far.[8] Similar behavior, including the formation of external E–E bonds upon oxidation, was reported for the complexes $[\{CpMo(CO)_2\}_2(\mu,\eta^2{:}\eta^2\text{-}E_2)]$ (E = P–Bi), which results for E = P, As in the formation of the complexes **C** and **D** (Scheme 1).[9]

Not only sandwich complexes with an E_n ligand as a lower deck show an instructive redox chemistry, but also homometallic triple-decker complexes with the corresponding E_n ligand as a middle deck. $[(Cp^RMo)_2(\mu,\eta^6{:}\eta^6\text{-}P_6)]$, for example, can be easily oxidized to $[(Cp^RMo)_2(\mu,\eta^6{:}\eta^6\text{-}P_6)]^+$ (**E**), retaining its initial triple-decker geometry in the solid state, whereas the *cyclo*-P_6 ligand in **E** tends to slightly distort in a bis-allylic manner.[10] Therefore, in contrast to the usual polypnictogen complexes, here, oxidations have the opposite effect, namely of elongating P–P bonds, but of also strengthening Mo–Mo bonds.

Intrigued by the diversity of the structural changes observed upon oxidation and/or reduction of the polypnictogen (E_n) ligand complexes, we were interested in using E_n ligand complexes that combine the features of triple-decker complexes and separated E_n units, and we were keen to explore whether the redox behavior follows the traditional pathway (oxidation: forming a bond; reduction: cleaving a bond) or whether new avenues to novel and structurally unprecedented products are opened. Therefore, we investigated the redox chemistry of the cobalt complexes $[(Cp'''Co)_2(\mu,\eta^2{:}\eta^2\text{-}E_2)_2]$ (E = P (**1**), As (**2**); Cp''' = 1,2,4-tri-(*tert*-butyl)cyclopentadienyl), which are easily accessible by the reaction of the toluene complex $[(Cp'''Co)_2(\mu,\eta^4{:}\eta^4\text{-}C_7H_8)]$ with white phosphorus or yellow arsenic on gram scale.[11]

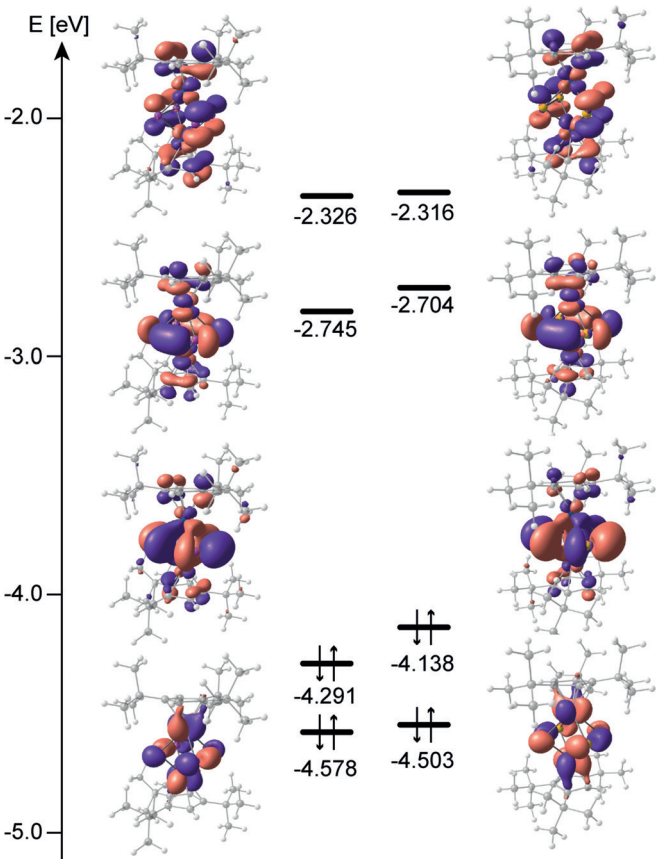

Figure 1. Frontier molecular orbitals of **1** (left) and **2** (right) at the BP86/def2-TZVP level of theory.

Results and Discussion

To gain first insight into their redox properties, the frontier molecular orbitals of **1** and **2** were computed (Figure 1). The HOMO shows bonding character within the E_2 units and antibonding character between them. Therefore, the abstraction of electrons by oxidation should induce a cyclization while the E–E distance of the former E_2 unit will be elongated. The situation for the LUMO, which is a linear combination of the π* orbitals of the E_2 units, is the other way around. The LUMO shows bonding character between the two separated E_2 units and antibonding character within the E_2 units. Again, the population of this orbital by adding electrons through reduction should induce a cyclization to form an E_4 ligand while the bond within each E_2 unit will be elongated.

To obtain an overview of how redox processes proceed, cyclic voltammetry measurements were performed in different solvents. We found that the nature of the redox process is strongly dependent on the solvent used. In the case of **1,** there are two reversible oxidation processes in CH_2Cl_2 at −367 and +351 mV and a, most likely, irreversible reduction around −2350 mV (vs. $[Cp_2Fe]/[Cp_2Fe]^+$). When the solvent is changed to THF, only one reversible oxidation at −336 mV and one reversible reduction at −2304 mV were observed (Figure 2). The cyclic voltammogram of **2** in DME shows two reversible oxidations at −463 and +8 mV and two reversible

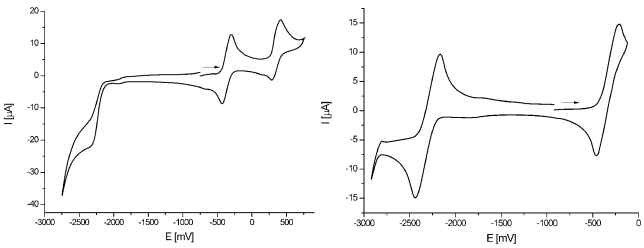

Figure 2. Cyclic voltammogram of **1** in CH_2Cl_2 (left) and in THF (right) vs. $[Cp_2Fe]/[Cp_2Fe]^+$ (electrolyte: $^nBu_4NPF_6$, scan rate: 100 mV s^{-1}, room temperature).

reductions at −2144 and −2644 mV vs. $[Cp_2Fe]/[Cp_2Fe]^+$ (see Figure 3).

For the chemical oxidation, we chose Ag^+ as a suitable oxidant, because of the rather low oxidation potentials of **1** and **2**.[12]

Both compounds can be oxidized by using one equivalent of an Ag^I salt containing a weakly coordinating anion [X] (X = BF_4 or [FAl]; [FAl] = $[FAl\{OC_6F_{10}(C_6F_5)\}_3]$) leading to the isostructural compounds $[(Cp'''Co)_2(\mu,\eta^4{:}\eta^4\text{-}E_4)][X]$ [E = P, X = BF_4 (**3a**; 66%), [FAl] (**3b**; 56%); E = As, X = BF_4 (**4a**; 65%), [FAl] (**4b**; 42%); Eq. (1)], in which two new E–E bonds have been formed to generate a new triple- decker sandwich complex with a cyclobutadiene-like formal E_4^{3-} middle deck.

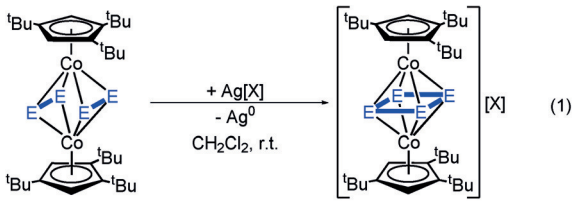

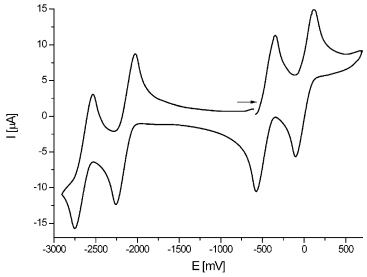

Figure 3. Cyclic voltammogram of **2** in DME vs. $[Cp_2Fe]/[Cp_2Fe]^+$ (electrolyte $N^nBu_4PF_6$, scan rate: 100 $mV\,s^{-1}$, room temperature).

Crystals suitable for single-crystal X-ray structure analysis were obtained from concentrated solutions in CH_2Cl_2, layered with pentane (**3b**, **4a**, **4b**) or hexane (**3a**) at −30 °C. As the compounds **3a**/**3b** and **4a**/**4b** are isostructural and differ solely in the used anion, only the structures of **3a** and **4a** in the solid state are depicted in Figure 4.

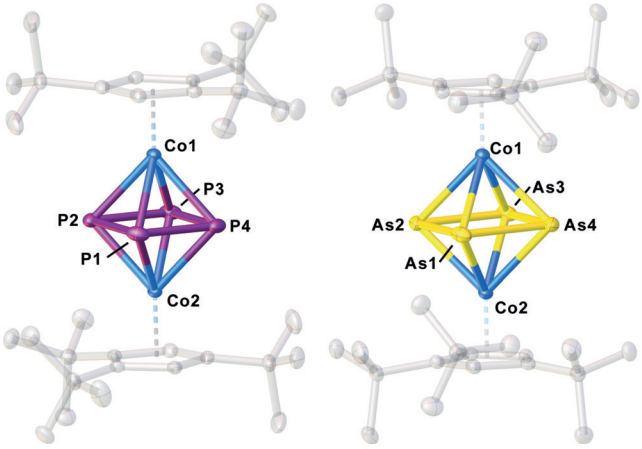

Figure 4. Structure of the cations in **3a** (left) and **4a** (right) in the solid state. Thermal ellipsoids set at 50% probability. Hydrogen atoms, anions and solvent molecules are omitted for clarity.

The structures reveal triple-decker complexes with *cyclo*-E_4 ligands coordinating in an $\eta^4{:}\eta^4$ fashion to two {Cp‴Co} fragments. The geometry of the *cyclo*-E_4 ligand is slightly distorted and differs a little in all compounds. For **3a** and **4a**, there are rectangular *cyclo*-E_4 ligands with two shorter E–E bonds (P1–P2 2.1860(9), P2–P3 2.1837(8), As1–As2/As3–As4 2.3882(2) Å) and two longer E–E bonds (P1–P4 2.3022(8), P2–P3 2.2960(8), As1–As4/As2–As3 2.5198(2) Å), which might be viewed as cyclobutadiene-like units. In **3b**, the E_4 ligand has a trapezoid shape with three shorter P–P bonds (P1–P2 2.2205(6), P2–P3 2.2358(6), P3–P4 2.2069(7) Å) and one longer one (P1–P4 2.3139(6) Å). In **4b**, the As_4 ligand is disordered over three positions with site occupancies of 5, 25, and 70%, preventing the accurate description of the As_4 unit.

DFT optimization of the geometries of **3a** and **3b** (BP86/def2-TZVP level of theory; **3a**^{c}, **3b**^{c}) revealed a rectangular E_4 ligand (similar to that observed in the crystal structure) for **3a** and a trapezoid-shaped ligand for **3b,** which is more widened than in **3b** (2.5133 Å (optimized geometry of **3b**^{c}) and 2.3139(6) Å (experimental structure of **3b**)). The geometry optimizations were both started from the atomic coordinates obtained from the X-ray structures. However, starting from a symmetric *cyclo*-P_4 ligand, this geometry is retained in the optimized structure of **3a**^{c}, the same as for the final trapezoid-shaped ligand in **3b**^{c}. The energy difference between the two isomers is only 3 $kJ\,mol^{-1}$, with the trapezoid isomer being favored. Both geometries represent minima on the energy hypersurface (see the Supporting Information). The structural differences between **3a** and **3b** can be attributed to packing effects as the counterions differ significantly in size. DFT calculations show a similar behavior for the arsenic compounds **4a** and **4b**. The formation of one P–P bond and the generation of a trapezoid-shaped ligand are reminiscent of the coordination of **1** to {$W(CO)_5$} fragments leading to ([(Cp‴Co)$_2$(μ,$\eta^4{:}\eta^4{:}\eta^1{:}\eta^1$-$P_4$){$W(CO)_5$}$_2$]).[13] However, in this complex, the P1–P2 and P3–P4 distances are significantly shorter (2.070(8) and 2.093(9) Å), the P2–P3 distance is quite the same (2.276(8) Å), and the P1–P4 distance is longer (2.962(8) Å) than the corresponding distances in **3b**. An analogous As compound is unknown.

The compounds **3a**/**3b** and **4a**/**4b** are paramagnetic. The ^1H NMR spectra in solution at room temperature reveal strongly shifted broad signals for the Cp‴ ligands. The EPR spectra (solid and in frozen solution at 77 K) show an isotropic resonance with the g_{iso} values indicating one unpaired electron each (77 K, solid: **3a**: $g_{iso} = 2.037$; **3b**: $g_{iso} = 2.024$; **4a**: $g_{iso} = 2.121$; **4b**: $g_{iso} = 2.094$; see the Supporting Information). The Evans NMR spectra reveal effective magnetic moments of 1.23 μ_B for **3b** and of 2.01 μ_B for **4b**, corresponding to about one unpaired electron each.

The pnictogen ligands in the starting materials **1** and **2** can be described as separated E_2^{2-} units (if Co^{III} moieties are assumed). Upon oxidation, one electron is removed, and formally, a *cyclo*-E_4^{3-} ligand is formed. The SOMO (**3a**: α-188, **4a**: α-224; see the Supporting Information) reveals that the unpaired electron is located mainly on the E_4^{3-} ligand (electron density within the short E–E bonds and between them with a minor contribution of the Co atoms, see the Supporting Information). The spin density is homogenously distributed over all E und Co atoms, and the absence of a hyperfine coupling to Co in the EPR spectra also underlines the presence of a formal *cyclo*-E_4^{3-} ligand. Likewise, the decrease in the formal charges (Mulliken charges, see the Supporting Information) of the E_4 ligand as compared to the starting complexes emphasizes this description. It has to be noted that this description of **3a** and **4a** is only a formalism as the electron density in the SOMOs is also distributed over

both Co atoms and the Cp‴ ligands, and the covalent character of the bonding between the E_4 ligand and the metal has to be considered.

Upon reacting **1** and **2** with Ag[TEF] ([TEF] = [Al{OC-$(CF_3)_3$}$_4$]), the dications $[(Cp'''Co)_2(\mu,\eta^4{:}\eta^4\text{-}E_4)][TEF]_2$ (E = P (**5**), As (**6**)) were obtained as crystalline compounds in yields of 68 and 69%, respectively [Eq. (2) in Figure 5], which now represent *cyclo*-E_4^{2-} middle decks with four equivalent bonds.

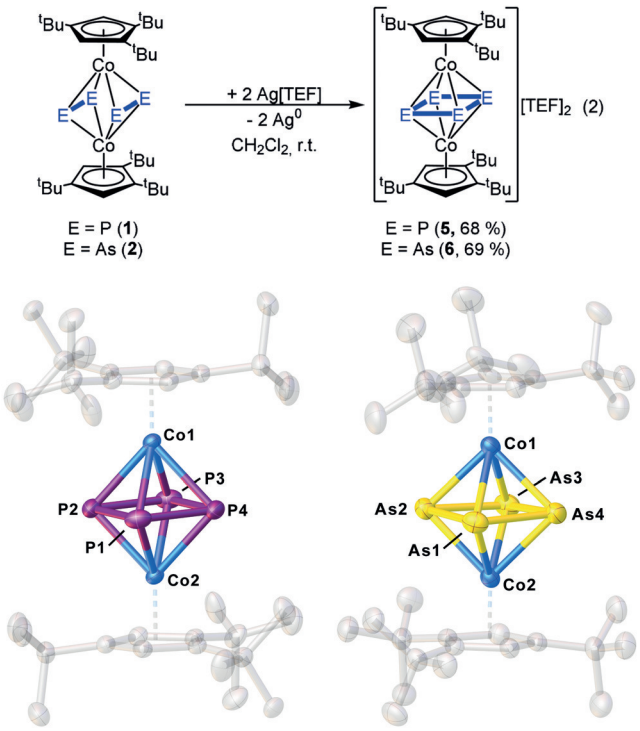

Figure 5. Structure of the dications in **5** (left) and **6** (right) in the solid state. Thermal ellipsoids set at 50% probability. Hydrogen atoms, anions, and solvent molecules are omitted for clarity.

The structures of **5** and **6** in the solid state (Figure 5) show triple-decker complexes with a *cyclo*-E_4 ligand as a middle deck. In **5**, the P_4 unit is planar with very similar P–P distances (2.236(2) and 2.239(2) Å) representing single bonds, which was confirmed by the Wiberg bond indices (WBI) of 0.92.[14] The P–P bonds in **5** are longer than those in the complexes with a *cyclo*-P_4 ligand as an end-deck as in $[Cp'''Co(\eta^4\text{-}P_4)]$ (2.1557(18)-2.1699(14) Å).[15] In contrast to **5**, the *cyclo*-As_4 ligand in **6** is slightly folded (fold angle 3°). The As–As bond lengths are between 2.4355(9) and 2.4759(9) Å and lie in the range of single bonds, as confirmed by WBIs between 0.80 and 0.93 (the DFT-optimized geometry reveals a trapezoid-shaped As_4 ligand with a fold angle of 6.4°).[14] The As–As distances are also longer than in complexes with a *cyclo*-As_4 ligand as an end-deck such as $[Cp^*Nb(CO)_2(\eta^4\text{-}As_4)]$ (2.345-(4)–2.409(4) Å).[16] The structural motif of the dication is reminiscent of the Cp^{tBu} ($C_5Me_4{}^tBu$)-substituted compound $[(Cp^{tBu}Co)_2(\mu,\eta^4{:}\eta^4\text{-}As_4)][Co_3Cl_8(thf)_2]$, obtained, however, by starting from $As_7(SiMe_3)_3$ as an As source.[17] This complex shows As–As distances of 2.4552(10) and 2.4680(11) Å. In the ^{1}H NMR spectrum of **5**, two broad singlets centered at δ = 1.82 and 1.71 ppm for the ^{t}Bu groups of the Cp‴ ligand can be detected, but no signals for the H atoms bonded to the Cp ring, indicating a dynamic process in solution. The $^{31}P\{^1H\}$ NMR spectrum at room temperature shows one broad singlet at δ = 494.0 ppm ($\omega_{1/2}$ = 4000 Hz). Upon cooling to −80 °C, the signals in the ^{1}H NMR spectra broaden further, and still no resonance for the Cp bond H atoms can be found. The signal in the $^{31}P\{^1H\}$ NMR spectra broadens too and eventually disappears completely. Upon warming an NMR sample of **5** in *ortho*-difluorobenzene containing a C_6D_6 capillary to 80 °C, the signals in the ^{1}H NMR spectra remained unchanged. In the $^{31}P\{^1H\}$ NMR spectrum, a singlet can be observed whose intensity decreases at 80 °C. In the ^{1}H NMR spectrum of **6**, three singlets centered at δ = 6.50, 1.66, and 1.50 ppm can be detected, with the signal for the Cp-bonded H atoms (6.50 ppm) being downfield-shifted by approximately 2 ppm in comparison to the starting material. Both **5** and **6** are EPR-silent.

The abstraction of another electron from the E_4^{3-} ligand in **3** and **4** leads to a further change in the geometry, and the ligand can now be described as a *cyclo*-E_4^{2-} unit. Identical P–P bonds in the completely planar middle deck of **5** indicate the presence of an aromatic P_4^{2-} ligand. The HOMO of **5** shows the electron density to be homogenously distributed over all P atoms (indicating four equivalent bonds) and both Co atoms (in the shape of a d orbital, see the Supporting Information). In the case of **6**, the As_4^{2-} ligand is not completely planar, and the As–As distances differ slightly from each other. The optimized geometry shows a trapezoid-shaped ligand with one side being more open than the structure in the solid state suggests. Therefore, the HOMO shows electron density within the three shorter As–As bonds and at the Co atoms (d orbitals). As the formal charges (Mulliken charges, see the Supporting Information) of the E_4 ligand in **5** and **6** decrease further compared to the monocations and relative to **1** and **2**, the formal description of the ligand as E_4^{2-} seems appropriate.

All mentioned oxidations of **1** and **2** are fully reversible. The addition of stoichiometric amounts of KC_8 selectively yields back the starting materials **1** and **2**. In the related cyclic voltammograms, both compounds **1** and **2** show reversible reduction processes at rather negative redox potentials. Potassium graphite was chosen as a suitable reducing agent. By using a small excess of > 1 equiv of KC_8, the monoanions $[K(18\text{-c-}6)(dme)_2][(Cp'''Co)_2(\mu,\eta^4{:}\eta^4\text{-}E_4)]$ (E = P (**7**), As (**8**)) can be obtained in crystalline yields of 56 and 40%, respectively, which now feature cyclobutadiene-like E_4^{5-} middle decks [Eq. (3)]. Because of their anionic character, **7** and **8** are extremely sensitive towards air and moisture.

The structures in the solid state (Figure 6) reveal a rectangular *cyclo*-E_4 middle deck for both compounds. Two shorter E–E bonds (P1–P2/P3–P4 2.1288(9), As1–As2/As3–As4 2.3074(16) Å) and two longer E–E bonds (P1–P4/P2–P3 2.3606(8), As1–As4/As2–As3 2.5852(15) Å) are present. All bonds are in the range of shortened and elongated single bonds, respectively, as also confirmed by the WBIs for the short (**7**: 1.18, **8**: 1.15) and long bonds (**7**: 0.68, **8**: 0.63).[14,18]

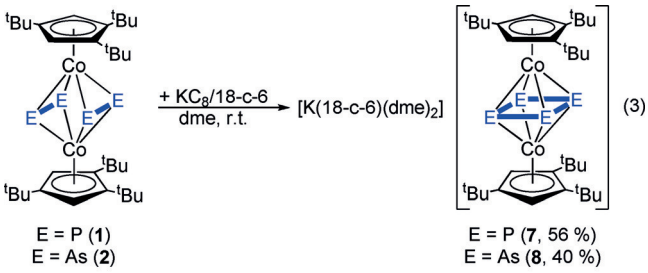

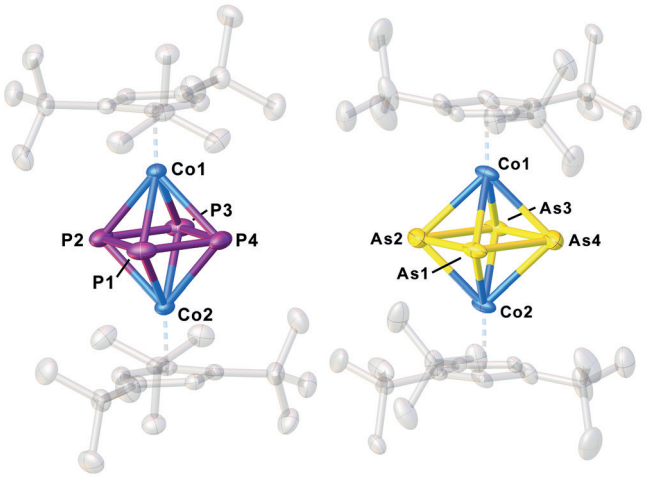

Figure 6. Structure of the anions in **7** (left) and **8** (right) in the solid state. Thermal ellipsoids set at 50% probability. Hydrogen atoms, cations, and solvent molecules are omitted for clarity.

Compounds **7** and **8** are both paramagnetic as indicated by the paramagnetic shift of the signals of the Cp‴ ligand in the ^{1}H NMR spectra in solution and by the absence of signals in the ^{31}P{^{1}H} NMR spectrum (for **7**). Both compounds are EPR-active and show resonances in solution (frozen solution) and in the solid state (at room temperature and at 77 K). The spectra of both compounds show a rhombically structured signal at 77 K in the solid state (**7**: $g_x = 2.0840$, $g_y = 2.0638$, $g_z = 1.9897$; **8**: $g_x = 2.2765$, $g_y = 2.0724$, $g_z = 2.0752$). The effective magnetic moment was determined by the Evans method to be 1.93 μ_B (**7**) and 2.35 μ_B (**8**), respectively, corresponding to about one unpaired electron each.

The DFT calculations reveal that the SOMO (**7**: α-189; **8**: α-225) is mainly located between E1–E4 and E2–E3 in a bonding fashion with some participation of a d orbital of the Co atoms and an antibonding π orbital of the Cp‴ ligands. The spin density is spread over the E_4 ligand and the Co atoms while being mainly located on Co, explaining the rhombic signals in the EPR spectra of **7** and **8**. The summed up Mulliken charges (see the Supporting Information) also indicate that the additional electron was transferred to the E_4 ligand and the formal description as E_4^{5-} moieties seems to be appropriate, although the spin density distribution indicates a partial charge delocalization also on the Co atoms and the Cp‴ ligands.

According to the cyclic voltammograms, **1** shows only one reversible reduction while **2** reveals two of them. Based on this observation, we attempted to access the doubly reduced product of **1**. Indeed, the reduction of **1** leads to the dianionic compound [K(18-c-6)(dme)$_2$][K(18-c-6)][(Cp‴Co)$_2$(μ,η^3:η^3-P_4)] (**9**), which was obtained in crystalline yields of 75% [Eq. (4)]. Probably, during the reaction, first the monoanion **7** is formed followed by a further reduction to the dianion **9**. The second reduction step occurs by cleavage of a P–P bond in **7** followed by rearrangement of the P_4 unit. Compound **9** is extremely sensitive towards air and moisture.

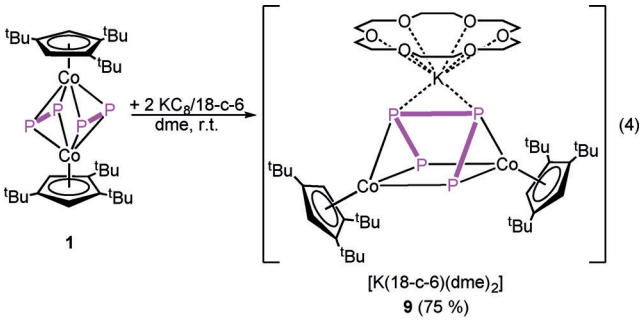

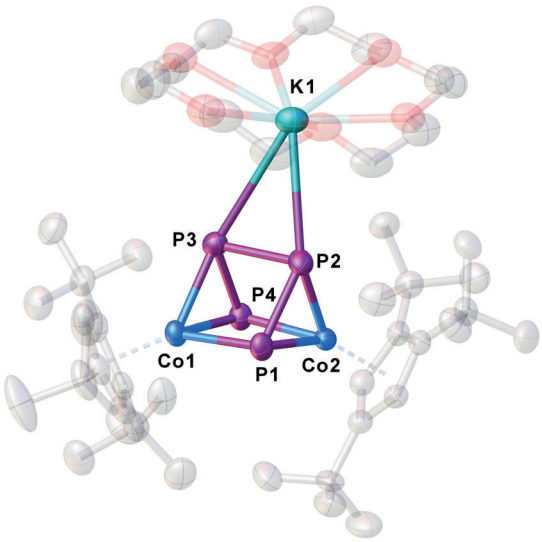

Figure 7. Structure of the dianion in **9** with one coordinating counter-ion in the solid state. Thermal ellipsoids set at 50% probability. Hydrogen atoms, the second cation, and solvent molecules are omitted for clarity.

The structure of **9** in the solid state (Figure 7) reveals a prismatic structural motif consisting of two {Cp‴Co} fragments and four P atoms. There are two shorter P–P bonds (P1–P2 2.1582(11), P3–P4 2.1615(11) Å) and one longer one (P2–P3 2.2646(10) Å). The P1···P4 distance is with 2.8396(12) Å too long for a P–P bond, but below the sum of the van der Waals radii ($\Sigma_{vdW} = 3.80$ Å).[19] Therefore, an interaction between the two nuclei can be expected. This is indeed confirmed by the WBI of 0.24. The P_4 ligand can be best described as being butadiene-like. The Co_2P_4 prismatic structural motif is reminiscent of the samarium complex [(Cp‴Co)$_2$(Cp*$_2$Sm)(μ$_3$,η^3:η^3:η^2-P_4)].[20] The $Co_2P_4^{2-}$ scaffold is also isoelectronic to the Ni_2P_4 unit in the complex [(Cp^{iPr}Ni)$_2$(μ,η^3:η^3-P_4)].[21]

In the $^{31}P\{^1H\}$ NMR spectrum of **9** in THF, two doublets centered at $\delta = 20.6$ and -7.5 ppm with a $^1J_{PP}$ coupling constant of 263 Hz can be assigned to the two inequivalent P atoms in **9**. The fact that the cyclic P_4 ligand in **7** rearranges upon addition of another electron is not obvious. The first step of the reaction would be formally a reduction to $[(Cp'''Co)_2(\mu,\eta^4{:}\eta^4\text{-}P_4)]^{2-}$ (**I-9a**). However, **I-9a** is 41.46 kJ mol^{-1} higher in energy than the anion of **9**. The coordination of a $[K(18\text{-c-}6)]^+$ unit to the edge of the P_4 ligand in **9** contributes with 193.73 kJ mol^{-1} to the stabilization of the product. Interestingly, when the potassium counterions were fully separated from the P_n ligand complex by using 2,2,2-cryptand instead of 18-c-6, no formation of **9** could be observed. Thus, by reacting **1** with an excess of potassium graphite in the presence of the 2,2,2-cryptand, only the monoanion **7** is obtained.

Both reductions of **1** and the reduction of **2** are fully reversible. The addition of stoichiometric amounts of $AgBF_4$ to **7**, **8**, and **9**, respectively, yields selectively the related starting materials. While the Co_2As_4 prism is known as a structural motif of the samarium compound ($[(Cp'''Co)_2(Cp^*_2Sm)(\mu_3,\eta^3{:}\eta^3{:}\eta^2\text{-}As_4)]$),[22] it cannot be obtained by the reduction of **2** with two equivalents of potassium graphite. Probably, an additional coordination to a Lewis acid such as Cp^*_2Sm is needed to obtain a stable compound. From the stoichiometric reaction, only the monoanion **8** can be isolated. By using an excess of potassium (fourfold or higher), one arsenic atom is abstracted, and $[K(dme)_4][(Cp'''Co)_2(\mu,\eta^3{:}\eta^3\text{-}As_3)]$ (**10**) can be isolated in crystalline yields of 26% [Eq. (5)]. In this reaction, the formation of a black precipitate is observed. Compound **10** is extremely sensitive towards air and moisture.

The structure in the solid state (Figure 8) reveals a bent triple-decker complex with an allylic As_3 ligand. The As1–As2 (2.4216(4) Å) and As2–As3 (2.4055(4) Å) bonds are in the range of single bonds, which was also confirmed by WBIs of 0.99.[14] The As1–As3 distance is 3.0224(5) Å, and too long to be considered as a bond. As the distance is still below the sum of the van der Waals radii ($\Sigma_{vdW} = 3.76$ Å), an interaction between the two atoms can be expected, which was confirmed by a WBI of 0.20.[19] Alternatively, **10** can be described as a nido cluster with a square-pyramidal Co_2As_3 core according to the Wade–Mingos rules. There are barely any triple-decker sandwich complexes known that include Cp ligands and a P_3 ligand as a middle deck, and none with an As_3 ligand. The Ni compounds $[(Cp'''Ni)_2(\mu,\eta^3{:}\eta^3\text{-}P_3)]^-$, $[(Cp'''Ni)_2(\mu,\eta^3{:}\eta^3\text{-}P_3)]$, and the heterobimetallic $[(Cp'''Co)(Cp'''Ni)(\mu,\eta^3{:}\eta^3\text{-}P_3)]$ have been reported.[23] While the nickel complexes formally possess one or two electrons more than **10**, the latter is isoelectronic to **10**. Therefore, **10** represents the first example of a triple-decker complex with an allylic As_3 ligand.

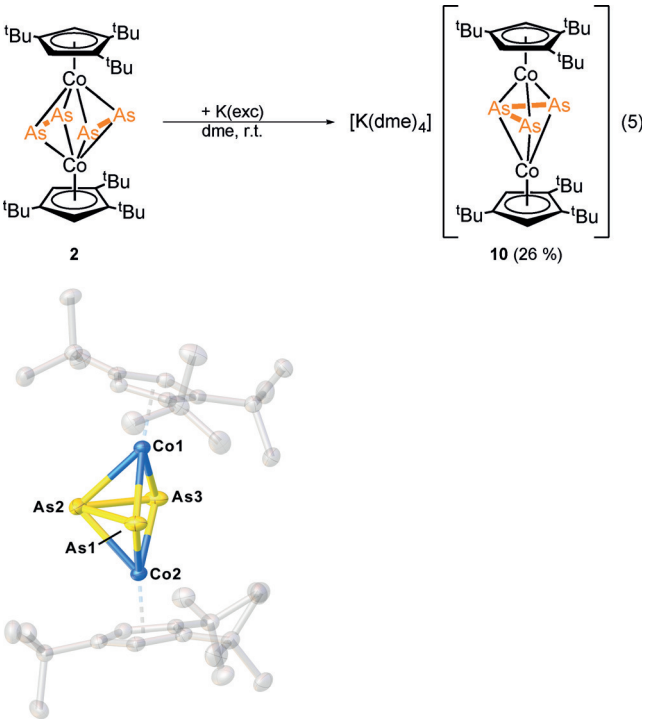

Figure 8. Structure of the monoanion in **10** in the solid state. Thermal ellipsoids set at 50% probability. Hydrogen atoms, cations, and solvent molecules are omitted for clarity.

Conclusion

We have shown that the cobalt complexes $[(Cp'''Co)_2(\mu,\eta^2{:}\eta^2\text{-}E_2)_2]$ (E = P (**1**), As (**2**)) exhibit a unique redox chemistry far from the usual behavior of a triple-decker complex or polypnictogen rings and cages. Instead, they display a distinctive platform where E–E bond formations can be performed using both oxidation and reduction reactions, with these processes being completely reversible. By reduction and oxidation, the two separate E_2^{2-} units in **1** and **2**, respectively, can be transformed into cyclobutadiene-like E_4^{3-} moieties (**3a**, **3b**, **4a**, **4b**) and E_4^{5-} moieties (**7**, **8**), respectively, or finally into *cyclo*-E_4^{2-} ligands in **5** and **6**. Further reduction of the monoanions **7** und **8** leads either to the cleavage of a P–P bond followed by rearrangement into a Co_2P_4 scaffold or, in the case of an $(As_2)_2$ unit, to the abstraction of one arsenic atom to yield a bent triple-decker complex with an allylic As_3 ligand as a middle deck (**10**), which represents the first example of a triple-decker complex with such a ligand. All redox processes (except for the formation of **10**) are fully reversible and can be selectively reversed when stoichiometric amounts of KC_8 or $AgBF_4$, respectively, are added. Even the formation of two P–P bonds as well as the cleavage of one P–P bond in the formation of **9** can be reverted stepwise upon addition of one or two equivalents of $AgBF_4$. Moreover, these results also clearly show the similarities and the different behavior of the $(As_2)_2$ entity in **2** and the $(P_2)_2$ moiety in **1** within these redox processes.

Acknowledgements

This work was supported by the Deutsche Forschungsgemeinschaft within the projects Sche 384/32-2 and Sche 384/36-1. M.P. is grateful to the Fonds der Chemischen Industrie for a PhD fellowship.

Conflict of interest

The authors declare no conflict of interest.

Keywords: arsenic · cobalt · cyclic voltammetry · phosphorus · redox chemistry

How to cite: *Angew. Chem. Int. Ed.* **2020**, *59*, 7154–7160
Angew. Chem. **2020**, *132*, 7220–7227

[1] a) G. Gnutzmann, F. W. Dorn, W. Klemm, *Z. Anorg. Allg. Chem.* **1961**, *309*, 210; b) M. Delamar, *J. Electroanal. Chem. Interfacial Electrochem.* **1975**, *63*, 339; c) G. Brauer, E. Zintl, *Z. Phys. Chem. Abt. B* **1937**, *37*, 323.
[2] a) T. Köchner, T. A. Engesser, H. Scherer, D. A. Plattner, A. Steffani, I. Krossing, *Angew. Chem. Int. Ed.* **2012**, *51*, 6529; *Angew. Chem.* **2012**, *124*, 6635; b) R. J. Gillespie, J. Passmore, P. K. Ummat, O. C. Vaidya, *Inorg. Chem.* **1971**, *10*, 1327.
[3] a) W. A. Henderson, M. Epstein, F. S. Seichter, *J. Am. Chem. Soc.* **1963**, *85*, 2462; b) S. Gómez-Ruiz, E. Hey-Hawkins, *New J. Chem.* **2010**, *34*, 1525; c) A. Tzschach, V. Kiesel, *J. Prakt. Chem.* **1971**, *313*, 259; d) M. Baudler, C. Gruner, G. Fürstenberg, B. Kloth, F. Saykowski, U. Özer, *Z. Anorg. Allg. Chem.* **1978**, *446*, 169.
[4] a) L. Cataldo, S. Choua, T. Berclaz, M. Geoffroy, N. Mézailles, L. Ricard, F. Mathey, P. Le Floch, *J. Am. Chem. Soc.* **2001**, *123*, 6654–6661; b) J. D. Hoefelmeyer, F. P. Gabbaï, *J. Am. Chem. Soc.* **2000**, *122*, 9054–9055; c) M.-E. Moret, L. Zhang, J. C. Peters, *J. Am. Chem. Soc.* **2013**, *135*, 3792–3795; d) Y. Canac, D. Bourissou, A. Baceiredo, H. Gornitzka, W. W. Schoeller, G. Bertrand, *Science* **1998**, *279*, 2080–2082; e) S. D. Grumbine, R. K. Chadha, D. Tilley, *J. Am. Chem. Soc.* **1992**, *114*, 1518–1520.
[5] O. J. Scherer, T. Brück, *Angew. Chem. Int. Ed. Engl.* **1987**, *26*, 59; *Angew. Chem.* **1987**, *99*, 59.
[6] R. F. Winter, W. E. Geiger, *Organometallics* **1999**, *18*, 1827.
[7] M. V. Butovskiy, G. Balazs, M. Bodensteiner, E. V. Peresypkina, A. V. Virovets, J. Sutter, M. Scheer, *Angew. Chem. Int. Ed.* **2013**, *52*, 2972; *Angew. Chem.* **2013**, *125*, 3045.
[8] M. Schmidt, D. Konieczny, E. V. Peresypkina, A. V. Virovets, G. Balázs, M. Bodensteiner, F. Riedlberger, H. Krauss, M. Scheer, *Angew. Chem. Int. Ed.* **2017**, *56*, 7307; *Angew. Chem.* **2017**, *129*, 7413.
[9] L. Dütsch, M. Fleischmann, S. Welsch, G. Balázs, W. Kremer, M. Scheer, *Angew. Chem. Int. Ed.* **2018**, *57*, 3256; *Angew. Chem.* **2018**, *130*, 3311.
[10] M. Fleischmann, F. Dielmann, G. Balázs, M. Scheer, *Chem. Eur. J.* **2016**, *22*, 15248.
[11] a) F. Dielmann, M. Sierka, A. V. Virovets, M. Scheer, *Angew. Chem. Int. Ed.* **2010**, *49*, 6860; *Angew. Chem.* **2010**, *122*, 7012; b) C. Graßl, M. Bodensteiner, M. Zabel, M. Scheer, *Chem. Sci.* **2015**, *6*, 1379.
[12] N. G. Connelly, W. E. Geiger, *Chem. Rev.* **1996**, *96*, 877.
[13] O. J. Scherer, G. Berg, G. Wolmershäuser, *Chem. Ber.* **1995**, *128*, 635.
[14] P. Pyykkö, M. Atsumi, *Chem. Eur. J.* **2009**, *15*, 186.
[15] F. Dielmann, A. Timoshkin, M. Piesch, G. Balázs, M. Scheer, *Angew. Chem. Int. Ed.* **2017**, *56*, 1671; *Angew. Chem.* **2017**, *129*, 1693.
[16] O. J. Scherer, J. Vondung, G. Wolmershäuser, *J. Organomet. Chem.* **1989**, *376*, C35–C38.
[17] C. von Hänisch, D. Fenske, F. Weigend, R. Ahlrichs, R. Ahlrichs, F. Weigend, *Chem. Eur. J.* **1997**, *3*, 1494.
[18] P. Pyykkö, M. Atsumi, *Chem. Eur. J.* **2009**, *15*, 12770.
[19] S. Alvarez, *Dalton Trans.* **2013**, *42*, 8617.
[20] T. Li, N. Arleth, M. T. Gamer, R. Köppe, T. Augenstein, F. Dielmann, M. Scheer, S. N. Konchenko, P. W. Roesky, *Inorg. Chem.* **2013**, *52*, 14231.
[21] O. J. Scherer, J. Braun, P. Walther, G. Wolmershäuser, *Chem. Ber.* **1992**, *125*, 2661.
[22] C. Schoo, R. Köppe, M. Piesch, M. T. Gamer, S. N. Konchenko, M. Scheer, P. W. Roesky, *Chem. Eur. J.* **2018**, *24*, 7890.
[23] a) E. Mädl, G. Balázs, E. V. Peresypkina, M. Scheer, *Angew. Chem. Int. Ed.* **2016**, *55*, 7702; *Angew. Chem.* **2016**, *128*, 7833; b) M. Piesch, F. Dielmann, S. Reichl, M. Scheer, *Chem. Eur. J.* **2020**, *26*, 1518.

Manuscript received: December 27, 2019
Revised manuscript received: January 28, 2020
Accepted manuscript online: February 3, 2020
Version of record online: March 13, 2020

